Energy & Environmental Science

ROYAL SOCIETY OF CHEMISTRY

PAPER

View Article Online
View Journal | View Issue

Cite this: *Energy Environ. Sci.*, 2022, **15**, 2545

Multisource energy conversion in plants with soft epicuticular coatings†

Fabian Meder, *[a] Alessio Mondini, [a] Francesco Visentin,[a] Giorgio Zini,[b] Marco Crepaldi[b] and Barbara Mazzolai*[a]

Living plants have recently been exploited for unusual tasks such as energy conversion and environmental sensing. Yet, using plants as small-scale autonomous energy sources is often impeded by multicable and -electrode installations on the plants. Moreover, insufficient power outputs for steadily driving even low-power electronics made a realization challenging. Here, we show that plants, by a modification of the leaf epicuticular region can be transformed into cable-free, fully plant-enabled integrated devices for multisource energy conversion. In detail, leaf contact electrification caused by wind-induced inter-leaf tangency is magnified by a transparent elastomeric coating on one of two interacting leaves. This enables converting wind energy into harvestable electricity. Further, the same plant is used as an unmatched Marconi-antenna for multi-band radio frequency (RF) energy conversion. This enables the use of the same plant as a complementary multi-energy system with augmented power output if both sources are used simultaneously. In combination, we observed over 1000% enhanced energy accumulation respective to single source harvesting in the specific application case and common plants like ivy could power a commercial sensing platform wirelessly transmitting environmental data. This shows that living plants have potential to autonomously supply application-oriented electronics while maintaining the positive environmental impact by their intrinsic sustainability and benefits such as O_2 production, CO_2 fixation, self-repair, and many more.

Received 4th February 2022,
Accepted 5th April 2022

DOI: 10.1039/d2ee00405d

rsc.li/ees

Broader context

Approaches to harness living plants for energy conversion and sensing are evolving and exploiting the materials and physiology of the organisms. Generating electricity with plants was recently achieved using wind, rain drops, the root microbiome, sap, temperature gradients by mechanisms like triboelectricity, glucose fuel cells, microbial fuel cells, Peltier elements *etc.* Yet, the systems may require complex artificial installations on plants or in their surroundings and the energy outputs are often not sufficient to sustain even low-power devices. Here, we describe a new approach for multisource energy harvesting with plants. By only slight modifications of the leaves with a thin, harmless silicone coating, we could convert wind energy into electricity through contact electrification of two interacting leaves. At the same time, the plant was used as ionic receiving antenna for multiband radiofrequency radiation. This enabled a second, complementary energy source and enhanced the power output. The plants could drive a commercial wireless temperature and humidity sensor showing the potential to autonomously supply application-oriented electronics while maintaining their positive environmental impact and intrinsic sustainability and benefits such as O_2 production, CO_2 fixation, self-repair, and many more.

[a] *Bioinspired Soft Robotics Laboratory, Istituto Italiano di Tecnologia, 56025 Pontedera, Italy. E-mail: fabian.meder@iit.it, barbara.mazzolai@iit.it*
[b] *Electronic Design Laboratory, Istituto Italiano di Tecnologia, 16152 Genova, Italy*

† Electronic supplementary information (ESI) available: Fig. S1. Circuit model used to estimate the behavior of two leaf generators on the same or separate plants. Fig. S2. Effect of the leaf coating on self-healing of wounded leaves. Fig. S3. Mechanical energy conversion by c–u leaf pairs. Fig. S4. Scanning electron microscopy images of the coated *H. helix* leaves and effect of coating thickness on the voltage output. Fig. S5. Mechanical-to-electrical energy conversion efficiency of a c–u leaf pair. Fig. S6. Influence of climber *H. helix'* support material on the mechanical energy conversion. Fig. S7. Model for the estimation of the behavior of signal generation and energy harvesting with multiple leaves on the same plant. Fig. S8. Influence of leaf-wetting on c–u leaf pair energy conversion. Fig. S9. Electric field characteristics and field strength-dependent energy harvesting using *H. helix*. Fig. S10. Effect of ion conduction obstruction by tissue drying on energy harvesting and impedance analysis. Fig. S11. Application scenario: Signals received during plant-based RF energy harvesting in an urban outdoor environment. Table S1. Overview of context of plant-hybrid energy harvesting and sensing techniques. Movie 1. Cable-free, leaf tangency-enabled wind energy conversion by living plants. See DOI: **https://doi.org/10.1039/d2ee00405d**

Introduction

Advances in the understanding of material properties, biochemical mechanisms, and physical processes in artificial and biological matter have shown that living organisms and especially living plants can be exploited for energy conversion[1–6] and environmental sensing[7–14] by interfacing and modifying the plants with engineered materials and electronics that enable to turn them into "devices".[15–18]

Plant-integrated solutions like light-emitting plants,[19] plant-hybrid sensing platforms,[7–14] plant-internal electronic circuits,[20,21] and plant-hybrid robotics,[22] as well as living plant-driven energy harvesting[1–3] using wind,[5,23] rain drops,[4] the root/soil microbiome,[24–27] sap components,[28–30] temperature gradients,[31] and potential differences between soil and plant[32] endow great prospects for connecting plants to man-made technology and for sustainable concepts to derive novel energy-autonomous devices, for example for environmental monitoring, in agriculture, climate change surveillance, ecosystem investigations *etc.* Table S1 (ESI†) gives an extended overview of approaches and principles of energy harvesting and sensing by plants and compares the output power of such devices.

Using plants as small-scale energy sources[1–5] is often impeded not only by insufficient power outputs for steadily driving even low-power electronics but also by installations on the plants that makes a realization challenging. Often, substantial modification of the plants is required such as by integrated systems like artificial leaves and multiple cables and specific species or maintaining certain conditions (*e.g.*, high soil humidity for plant microbial fuel cells, assuring catalytic activity for glucose fuel cells *etc.*). Plants continuously change their morphology by growing at their apical regions and by exchanging leaves. Hence, preserving complex artificial components in plants is a challenging issue and environmentally questionable on a larger scale.

Consequently, approaches that augment the overall power output not only relying on a single energy conversion mechanism as well as approaches that require minimal alteration of the plants by further integration and elimination of external components as best as possible are required to fully derive the potential to use living plants in hybrid energy harvesting.

Here, we show for the first time that life plants can convert multiple energy sources into electricity that is wind energy and RF energy. The energy thereby harvested can autonomously power a commercial sensing platform even outdoor. The combination of several independent energy sources not only gives the opportunity to augment the power output but leads also to the possibility of a complementary multi-energy system, that remains operable also when a single source, *e.g.*, wind is momentarily not available.

We modify plant leaves with a micro-scale epicuticular coating consisting of a transparent elastomeric layer applied on the upper leaf side that can be easily administered by coating or potentially by spraying (similar to, *e.g.*, pesticide application or by newer technologies like drones[33]).

The coating does not harm the plant or inhibit intrinsic processes like photosynthesis. After coating, the leaves capability of producing high charge imbalances on their surfaces by contact electrification is strongly increased. This occurs for example when the coated leaf touches another uncoated leaf driven by wind. The charges can be harvested by a single electrode in the plant stem.

Different from previous prototypes,[5] in which we installed an artificial leaf containing a silicone-coated electrode on top of the natural leaf, here, the silicone layer is integrated on the leaf and the tissue of two interacting plants act as electrodes. The leaf coatings are simple to apply and more complex electrodes, installations in the tissue, in the soil, or the trunk as needed by many methods described in Table S1 (ESI†) are not required.

Moreover, we show for the first time that multi-frequency band RF energy conversion can be coupled using the plant as an unmatched Marconi-antenna and the same single harvesting electrode as for wind energy conversion can be used to harvest the electricity. The data shows that the unique combinatory use of wind and RF energy by the same living plant strongly enhances the energy accumulation respective to single source harvesting. We interfaced a commercial sensing platform with the plants and power it outdoor using existing plants in an urban environment to drive the sensor platform and wirelessly transmitting environmental data.

This shows that living plants could autonomously supply application-oriented electronics while maintaining their own positive environmental impact[34] by their intrinsic benefits such as O_2 production, CO_2 fixation, self-repair, and many more extremely difficult (if at all possible) to realize in artificial harvesters.

Experiments and methods

Plant species

F. microcarpa (height h = 25 cm), large *H. helix* (h = 120 cm), small *H. helix* (h = 35 cm) were purchased at a local plant nursery. The plants were kept in a phytochamber controlled at 50–60% relative humidity (RH), a temperature of 25 °C, and a light exposure of a 16 hours day and 8 hours night cycle, watered twice per week, and fertilized once per month with a green plant fertilizer. Outdoor experiments with common urban vegetation, *i.e.*, *H. helix*, *P. pinea*, *Y. elephantipes*, and *P. peltatum* were performed during the period of May 2020 to February 2021 in the front yard of a multifamily residence in a suburb of Pisa, Italy. *H. helix* (h = ~8 m) grew naturally on the stem of a ~15 m high *P. pinea* tree and *Y. elephantipes* (h = 2.5 m) grew in a distance of about 4 m from the *P. pinea*. *P. peltatum* (h = 25 cm) was potted in isolated PVC pottery fixed on the balcony balustrade of the residence in a height of 7 m.

Materials and procedure for epicuticular coating

The adaxial surface of leaves attached to the plants was coated with a low viscous, translucent silicone elastomer prepolymer (Ecoflex 0030, Smooth-On Inc., USA) using a brush leading to a thin layer on the leaves. Excess precursors were left to drop off the leaf. The coatings were cured at 25 °C, 60% RH for 24 hours resulting in epicuticular coatings of ~10 mg cm^{-2} polymer per leaf area and a typical thickness of ~100 μm.

Pre- and post-coating transpiration analysis

Whole plant transpiration analysis pre- and post-coating was performed during a three-day period in a transparent, gas tight chamber equipped with internal CO_2 and humidity sensors (SCD30, Sensirion AG, Switzerland, sampling rate 2 s) which was placed in a grow room with a 16 hours day and 8 hours night lighting cycle. External CO_2 and humidity sensors (SCD30, Sensirion AG, Switzerland, sampling rate 2 s) served as reference.

Setup for controlled mechanical and air-flow stimulation of c–u and u–u leaf pairs

To apply controlled mechanical stimuli between c–u (coated–uncoated) and u–u (uncoated–uncoated) leaf pairs, a previously described setup consisting of a linear actuator (4Ω HiFi full-range driver, diameter 8 cm, model FRS, Visaton, Germany) driven by a monolithic power amplifier (OPA549T, Burr-Brown, USA) controlled by a function generator (GFG-8217A, GW Instek, Taiwan) was used to create a vertical motion used to stimulate the leaves selecting waveform, frequency, amplitude, and offset.[1] A load cell (LRF400, FUTEK Advanced Sensor Technology, Inc., USA) was used to record the impact force during the multicycle contact-release stimuli. Different impact forces were adjusted by lowering or increasing the distance between the leaf pairs during stimulation using a motorized stage in steps of 10 μm (DC-3K, Controller MS 314, Märzhäuser GmbH & Co. KG, Germany). The measurements were conducted in a Faraday cage under ambient conditions (temperature typically 22 °C and 50% RH). To simulate wind, an air flow was created by a brushless cooling fan with an outlet diameter of 4 cm in a distance of about 40 cm from the leaf pairs under investigation. Air flow was controlled by adjusting the fan's supply voltage and resulting wind speeds were measured using a hot wire anemometer (405i, Testo SE & Co. KGaA, Germany) at a distance of ~2 cm in front of the leaf.

RF sources and controlled exposure

During in- and outdoor experiments, the plants were exposed to ambient RF radiation emitted from, *e.g.*, radio stations, building supplies, telecommunication *etc.*

For in depth analysis of RF harvesting, the plants were exposed to a controllable, on/off-switchable RF source constituted by the fluorescent lighting system in the plant grow room consisting of 128 fluorescent lamps (MASTER TL5 HO 54W/840, Philips, The Netherlands) that generated a ~390 kHz centre frequency RF signal received by the plants during the experiments when turned on.

The generated electric field was analysed in detail in terms of field strength and radiated power as function of distance from the source (Fig. S9, ESI†). Faraday caging made of plain square weave copper mesh with a density of 6.3 strands per cm (PSY406, Thorlabs, Germany) was used to shield RF radiation.

Voltage and current measurements

Gold coated metal pin electrodes (0.2 mm) were inserted into the plant tissue for electrical measurements (at the petiole for single leaves and in the stem for whole plants).

Short circuit currents were measured using a high input impedance electrometer (6517B, Keithley, USA) and voltages with an oscilloscope (MSO7014A, Agilent Technologies, USA) with a passive 100 MΩ input impedance probe (TT-HV 150, Testec GmbH, Germany).

Voltages over capacitors were recorded either by a data acquisition hardware (USB-6216, National Instruments, USA) or the electrometer (6517B, Keithley, USA). The plants were connected using coaxial cables (SMA RG142U, RS PRO, UK) to avoid interference of the cables on data acquisition.

Spectrum analysis

Spectrum analysis was performed using a spectrum and network analyser with a frequency range from 9 kHz to 3.2 GHz (SVA1032X, Siglent Technologies, Germany). The plants were connected using coaxial cables (SMA RG142U, RS PRO, UK) by connecting the central pin to the pin electrode penetrating the plant tissue at the base of the stem.

Electric field analysis

Electric field strength and power was measured using a laser-powered, high-speed, low-noise 3D electric field probe operating in a frequency range from 10 Hz–8.2 GHz (LS Probe 1.2, LUMILOOP, GmbH, Germany).

Impedance spectroscopy

Impedance spectroscopy was performed in freshly cut branches of *H. helix* applying a 1 V bias between two pin electrodes inserted in the inner tissue at the indicated distances and frequencies using the precision LCR Meter (E4980A, Keysight Technologies, USA).

Energy harvesting circuits, sensing, and wireless data transmission

The components for assembling the energy harvesting, sensing and data transmission circuits were low leakage diodes (BAS416, Nexperia, The Netherlands), ceramic capacitors (Taiyo Yuden Co. LTD, Japan) with indicated capacitances, and the temperature and humidity sensing and 868 MHz RF transmitter module (STM 330 & HSM100, EnOcean GmbH, Germany) of which the solar cell, battery, and capacitor were removed and replaced with a 136 μF capacitor connected to the plants using the indicated circuits for energy harvesting, sensing, and data transmission. The plants were connected using coaxial cables (SMA RG142U, RS PRO, UK) by connecting the central pin to the pin electrode penetrating the plant tissue at the base of the stem.

Simulation of multiple leaf energy harvesting circuit

Circuit simulation to estimate requirements for electrical insulation between two leaves to obtain a positive power balance during energy harvesting was done in Matlab/Simulink (Version R2019b) using the circuit depicted in Fig. S1 (ESI†) and assuming a tissue resistance of 100 kΩ and a 10 V, 5 Hz sinusoidal alternating voltage signal generated by the leaves.

The analysis of the sum signal of multiple overlapping signals randomly generated by multiple leaves was done in

Matlab using a code that builds the cumulative sum of a given number of input current signals simulated by a Neuron spike model[35] as further described in Fig. S7 (ESI†).

Further instrumentation and methods

Leaf surfaces and manually cut cross-sections of leaves with epicuticular coatings were imaged with a digital microscope (KH-8700, Hirox, USA). Transmission spectra of epicuticular coatings were measured in a UV-Vis spectrophotometer (Lambda 45, PerkinElmer, USA). The *H. helix* support panel was cut from 5 mm PMMA sheets using a laser cutter (Versa-Laser VLS2.30, Universal Laser Systems, Austria).

Analysis of the mechanical energy conversion efficiency

To estimate the efficiency to convert mechanical energy applied to a c–u leaf pair $E_{\mathrm{mech,in}}$ into electrical energy E_{out} after epicuticular coating, we analyzed the instantaneous conversion efficiency $n_{\mathrm{M,overall}}$ of the c–u leaf contact based on equation (1)

$$n_{M,\mathrm{overall}}(\%) = \frac{E_{\mathrm{out}}}{E_{\mathrm{mech,in}}}100 = \frac{\int_{t_{\mathrm{c,on}}}^{t_{\mathrm{c,off}}} I(t)^2 R_{\mathrm{L}}\,\mathrm{d}t}{mgL(1-\cos\theta)}100 \quad (1)$$

where I is the current produced by the c–u leaf pair, R_{L} is the load resistance (here 10 MΩ or 100 MΩ, respectively), the potential energy $E_{\mathrm{mech,in}} = mgL(1-\cos\theta)$, where m is the mass (here 32 g) with the dimension of 1 cm^2 onto which an uncoated leaf was fixed.[36] The mass and leaf were fixed on a friction less pendulum of length L that was dropped from varying heights at an angle θ onto a coated leaf supported by a rigid surface (g is the gravitational acceleration). Currents across the two leaves connected through R_{L} during the peak interval from $t_{\mathrm{c,on}}$ to $t_{\mathrm{c,off}}$ measured by an electrometer were used to calculate E_{out}.

Analysis of capacitor charging dynamics by plant converting environmental RF energy

To estimate the efficiency n_{RF} of the plants charging the capacitor by converting RF energy at the specific given conditions, we considered the power balance between the RF input power $P_{\mathrm{RF,in}}$ and the maximal power transfer to a load (capacitor) considering the global maximum of the instantaneous power charging the capacitor $P_{\mathrm{cap,charging}} = \frac{C\Delta V^2}{2\Delta t}$ using the eqn (2)

$$n_{\mathrm{RF,overall}}(\%) = \frac{P_{\mathrm{cap,charging}}}{P_{\mathrm{RF,in}}}100 \quad (2)$$

where C is the capacitance, t is the time after which V over the capacitor was reached, and $P_{\mathrm{RF,in}} = \sqrt{P_x^2 + P_y^2 + P_z^2}$ where P_x, P_y, P_z are the x-, y-, and z-components of the electric field power averaged over the full plant height in z direction, measured in the vicinity of the plant by an electric field probe.

The short circuit current related to capacitor charging was calculated by eqn (3) for $t \rightarrow 0$ and capacitor initially discharged.

$$I_{\mathrm{SC,cap}} = \lim_{t\to 0} C\frac{\mathrm{d}V}{\mathrm{d}t}; \quad V_{(0)} = 0 \quad (3)$$

and the load equivalent was estimated by eqn (4)

$$R_{\mathrm{e}} = \frac{\Delta V}{\Delta I} \quad (4)$$

to determine the load at which the maximal instantaneous power $P_{\mathrm{cap,charging}}$ was transferred.

To estimate the conversion efficiency of the RF harvesting circuit n_{circuit} under the specific conditions of the experiment, the power balance between and the maximal power transfer to the load (capacitor) considering the global maximum of the instantaneous power charging the capacitor $P_{\mathrm{cap,charging}}$ and the power received by the plant, P_{SA}, was considered, eqn (5)

$$n_{\mathrm{circuit}}(\%) = \frac{P_{\mathrm{cap,charging}}}{P_{\mathrm{SA}}}100 \quad (5)$$

Here, P_{SA} is the average power of RF signals received by the plant with RF source turned on. The power of RF signals received by plant was measured by the spectrum analyzer.

Analysis of increase of energy harvested by plant multimodal energy harvesting

A factor $f_{\mathrm{E,increase}}$ representing the energy rise by multimodal (RF + mechanical/wind) energy harvesting compared to single mode harvesting was calculated by (6):

$$f_{\mathrm{E,increase}}\frac{\Delta E_{\mathrm{multimode}} - \Delta E_{\mathrm{singlemode}}}{\Delta E_{\mathrm{singlemode}}} = \frac{\left(\frac{1}{2}C\Delta {V_{\mathrm{WRF}}}^2\right) - \left(\frac{1}{2}C\Delta {V_{\mathrm{S}}}^2\right)}{\frac{1}{2}C\Delta {V_{\mathrm{S}}}^2} \quad (6)$$

where $V_{\mathrm{W,RF}}$ is the voltage over capacitor harvested by wind and RF stimuli and V_{S} is the voltage over the capacitor when a single energy source (RF or mechanical) is converted by the plant into electrical energy. The variation of $E_{\mathrm{singlemode}}$ and $E_{\mathrm{multimode}}$ during 10 min capacitor charging (in intervals of 30 ms) have been considered.

Charges required for the sensing and wireless transmission cycle

In order to estimate the charges required for a measurement cycle Q_{meas} (charge required for sensing the humidity and temperature and wirelessly transmitting the data to the receiver), the variation in the voltage $V_{\mathrm{cap,sensor}}$ across the capacitor with capacitance C during a measurement cycle was analyzed in the corresponding time interval using eqn (7):

$$Q_{\mathrm{meas}} = C\left(V_{\mathrm{cap,sensor}}(t_1) - V_{\mathrm{cap,sensor}}(t_2)\right) \quad (7)$$

where t_1 and t_2 are the timepoints of begin and end of the measurement cycle, respectively.

Statistical methods

Information on data acquisition and statistics are given in the figure captions. Typically, the datapoints or curves represent mean and standard deviations of at least 3 measurements, some experiments were performed with up to 200 measurements per data points. All other experiments have been

repeated multiple times, when single measurement data is shown, it is representative. The statistical analysis was done in MATLAB (Version 2019b).

Results and discussion

Concept of plant-enabled multisource energy harvesting by epicuticular coatings

Our approach consists in modifying plants with the least possible, μm-scale variation rendering them capable of producing significant electrical outputs from wind-induced leaf movements and plant-antenna-based RF energy conversion. Fig. 1a gives an overview of the plant's simplified electrical structure exploited: the dielectric and purely polymeric cuticular membrane on the leaf surface and the ion-conductive inner cellular tissue and vascular system. Mechanical contact between the cuticle and another material generates charges on the cuticle by contact electrification which are electrostatically induced into the tissue acting as electrode as detailed in our previous investigation.[1]

Here, for the first time, the contacts of two leaves of two plants standing side-by-side is exploited to realize wind energy conversion. However, given by the well-recognized rules of contact electrification,[37–39] two similar materials (M1 = M2) such as two cuticles of unmodified leaves would generate insufficient charges for energy harvesting. The naturally similar lipids and waxes[40] in the plant cuticle form a material pair that does not enhance contact electrification. However, by tuning the materials (M1, M2) of the interacting cuticles, higher charging can be achieved. Hence, our approach consists of integrating a thin epicuticular dielectric layer on the leaf cuticle.

Silicone elastomers were tested previously to be one of the best counter materials for contact electrification of plant leaves leading to highest voltage signals generated.[1,3] Moreover, silicones have further advantages like their transparency, softness, and ease of application as a coating not affecting the living leaf and its physiology like transpiration as detailed below.

Fig. 1b illustrates a simplified circuit used to predict the behaviour of a coated leaf when transiently touching an uncoated leaf such as during wind fluttering (circuit model used for this simulation is given in Fig. S1, ESI†).

During transient mechanical contact, the two leaves generate a corresponding alternating current (AC) of opposite polarity (Fig. 1c). Yet, when R_{Soil} is low, charge separation is not possible as the internal plant-soil-plant circuit would inhibit charge separation and the signals compensate each other. The equivalent occurs, when two leaves on the same plant touch each other as the intrinsic tissue resistance does not provide sufficient isolation of the two leaf electrodes (Fig. 1d). However, when R_{Soil} is high enough to electrically isolate the two leaf electrodes (the model suggests $>10^8$–10^9 Ω), the charges generated can be separated and effectively harvested from both leaves (Fig. 1c).

High R_{Soil} were here simply achieved by potting plants in isolated pots (common plastic-based pottery) and this can possibly also be obtained in dry soil, or for example by placing harvesting electrodes closer to the leaves and maintaining long distances between leaves and roots/soil.

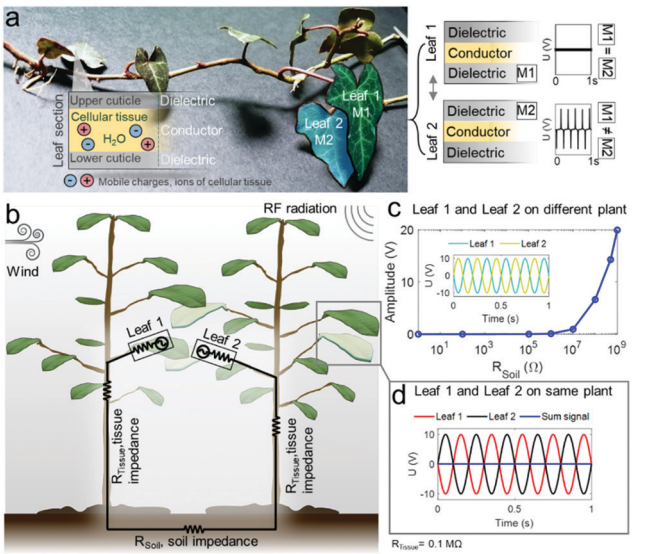

Fig. 1 Overview and model of living plant-based multisource energy harvesting. (a) Inner cellular and vascular tissue are ionic conductors; the cuticle on the plant surface is a dielectric polymeric layer onto which a silicone elastomer coating is applied. When a leaf with epicuticular coating comes in contact with an uncoated leaf, contact electrification generates considerable voltages U in the tissue if the dielectric material M1 and M2 specifically enhance contact electrification, typically M1 ≠ M2 here realized by coating with silicone elastomers. (b) Illustration of basic circuitry established by the plants in a wind and RF energy harvesting scenario. (c) Circuit simulation reveals that during mechanical interaction of two leaves from different plants, voltages in the tissue build up only when R_{Soil} is sufficiently high (see also Fig. S1, ESI†). (d) Signals of the two leaves cancel out when the leaves are on the same plant as electrical connection through the tissue (typical impedances ~0.1–1 MΩ) inhibit charge separation.

Effect of epicuticular coatings on plant transpiration, growth, and its enhancement of mechanical energy conversion

We then selectively deposited thin epicuticular silicone coatings (~10 mg cm^{-2}, on average 94 ± 16 μm thick) on the model species *Ficus microcarpa* (Fig. 2a), small plants with mechanically robust leaves that can be used in a laboratory setup. The coatings were applied on the adaxial surface of leaves with less stomata compared to the abaxial surface (Fig. 2b).

We analyzed the plant's transpiration and viability after the entire foliage was coated observing its growth in a 1 year-period and by measuring whole-plant level CO_2 and H_2O transpiration rates during several day-night cycles (Fig. 2c–e). The results reveal that even coating the entire foliage, did not obstruct transpiration and growth capabilities. Moreover, the foliage did not fall off or change color and growth of new leaves and branches was observed. Thus, the coating did not affect plant's viability and normal development (see new leaf and branch development in 1 year-growth-period Fig. 2c). This is also supported by the fact that the thin, soft, adaptive, and semi-permeable coatings allow high light transmission at wavelength regimes essential for leaf photosynthesis (Fig. 2e).

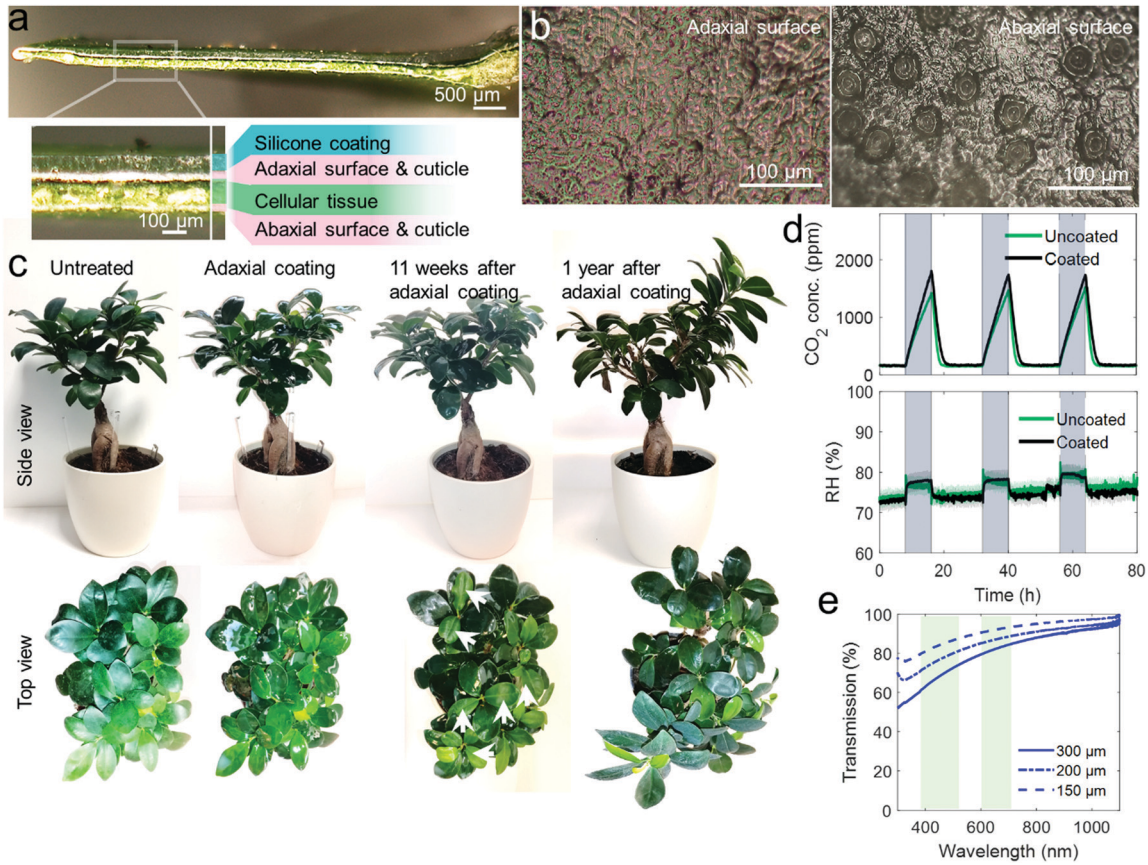

Fig. 2 Leaf-epicuticular coating and influence on plant viability. (a) Cross-section of *F. microcarpa* leaf with ~100 µm epicuticular silicone rubber coating on adaxial surface. (b) Microscopy images representing stomatal density on adaxial and abaxial leaf surface. (c) One-year growth observation of a fully coated *F. microcarpa*. White arrows point to new leaves that developed within 11 weeks after coating growing further into new branches within 1 year. (d) CO_2 and H_2O transpiration (in RH%), respectively before and after epicuticular coating of all leaves of a *F. microcarpa* plant observed for three days. (e) Light transmission of epicuticular coatings as function of its thickness, green bars highlight photosynthesis relevant wavelengths.

Moreover, we investigated the coating's effect on the self-healing[41] properties of plants after wounding the leaves and there was no significant adverse effect found as both, coated and uncoated leaves, remained alive after wounding (Fig. S2, ESI†).

Fig. 3a and b show the strong increase in the voltage amplitudes created when two leaves of two individual *F. microcarpa* plants touch each other as function of impact force and frequency, respectively. Signals were measured by a single pin-electrode in the stem at a distance of ~15 cm of the stimulated leaves. The combination of a single coated and uncoated leaf (c–u pair) generates voltage amplitudes of up to 25 V whereas the contact between uncoated–uncoated leaves (u–u pair) show signals in the mV range (details in Fig. S3a–c, ESI†). The values correspond to a 450 times increase in the generated potential difference for c–u pairs compared to u–u pairs. The current generated by a single c–u pair reaches an amplitude of 0.75 µA (Fig. S3d, ESI†).

Fig. 3c shows an arrangement of two plants in separate pots used to test voltage generation during air-flow/wind-excitation. Therein a c–u and a u–u leaf pair is realized at the position where both plants overlap. Only the c–u pair expectedly produced substantial voltages with amplitudes up to ~20 V when exposed to air-flow (Fig. 3d). Moreover, the output voltages scale with the wind speed (Fig. 3e) which bears a potential for an air-flow sensing capability. The contact of just two leaves in such a configuration can already charge a 10 µF capacitor in wind-susceptive manner (Fig. 3f).

Transfer of the concept to a climbing plant species, wind energy harvesting, and power analysis

For proving that the effect can be transferred to other species and to analyse a plant type that is especially interesting for urban ecosystems, *e.g.*, for vertical plant growth and greening of buildings,[42] we modified the climber *Hedera helix* (ivy).

Epicuticular coatings were applied on multiple leaves of two intertwining plants grown in separate pots to obtain c–u pairs (Fig. 4a). The adaxial leaf surfaces with less stomata were coated (Fig. 4b).

Fig. S4a (ESI†) shows scanning electron microscopy images of sections of the coated leaves showing the conformal attachment of the silicone layer to the upper leaf surface.

The generated voltage amplitude of c–u pairs scales with the impact force as well as the effective contact area reaching now even up to ~50 V for single leaves (Fig. 4c and d, respectively with 2 cm^2 contact area and 1 N impact force). The coating

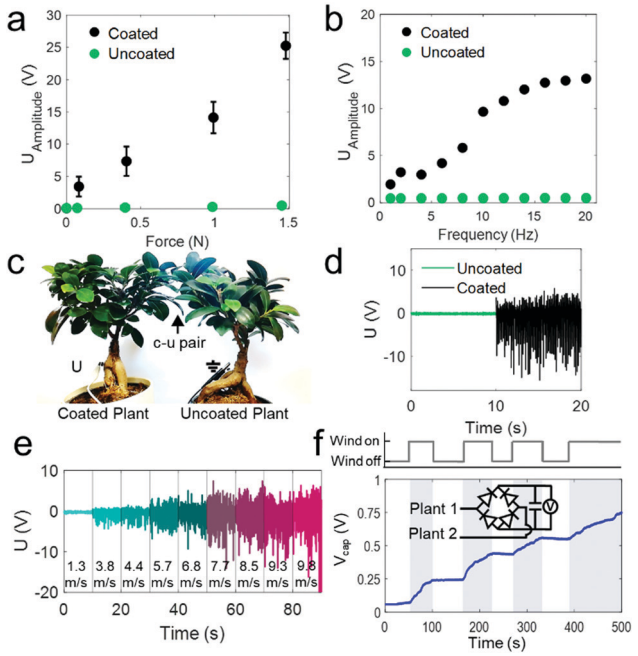

Fig. 3 Effect of leaf-epicuticular coating on enhancement of mechanical energy harvesting. (a) and (b) Enhancement of voltage generation after epicuticular coating as function of impact force (@10 Hz frequency), and of frequency (@1 N impact force), respectively in u–u and c–u leaf pairs. Data points and error bars represent mean and standards of 200 impacts on 5 leaves per force and frequency tested. Error bars in (b) are smaller than the symbol size. (c) Two *F. microcarpa* (left, coated, right uncoated) in separate pots and overlapping leaves (c–u pair) used for wind energy harvesting. (d) Air-flow induced voltage generation of a single u–u and c–u *F. microcarpa* pair. (e) Voltage generation as function of windspeed of a single c–u *F. microcarpa* pair. (l) c–u *F. microcarpa* leaf pair-based capacitor charging (10 μF) with indicated circuit as function of wind source on–off switching.

thickness may be further tuned to improve the voltage generation as indicated by the results in Fig. S4b (ESI†) which suggest an optimum at a thickness of ~130 μm. The power analysis of the system (Fig. 4e) reveals a peak power at 17 μW per cm^2 effective contact area between the two leaves (determined at 1N stimulus considering peak voltage and peak current measured when matching load impedance and internal impedance of the generator at 200 MΩ). These values are similar to those achieved with plant-hybrid systems[1,5] and many common triboelectric and piezoelectric generators[43–45] in particular at low impact forces. This shows that the combination of the epicuticular coatings and the whole plant as a circuit is competitive with minimal fabrication effort and can even convert low forces ≤1 N into harvestable electricity.

The mechanical-to-electrical energy conversion efficiency of a c–u pair is even higher at lower forces reaching values of 0.14% depending on the mechanical energy introduced (see energy conversion efficiencies of c–u pair at different conditions in Fig. S5, ESI†).

Indeed, the energy harvested from a single c–u pair is sufficient to supply a commercial temperature sensor with wireless transceiver connected to the plant using the circuit in Fig. 4f. The charging curve of the 136 μF capacitor driving the sensor during c–u pair excitation (1 N, 30 Hz) is depicted in Fig. 4g along with the wirelessly transmitted data and received signal strength.

The whole-plant *H. helix* (Fig. 4h) is also capable of converting wind energy into electricity. Fig. 4i shows the correlation of the voltage signal with the distance variation Δd between two leaves in a c–u leaf pair fluttering at a wind speed of ~8 m s^{-1} (Video 1 shows the fluttering motions of c–u pairs leading to signal generation in *H. helix* and *F. microcarpa*). The data confirms that the transient contact-and-release events caused by the leaf oscillations lead to the corresponding voltage signals. As the analysis showed that the output is also force- and contact area-dependent, the system is likely more effective, the more leaves are used and the higher the kinetic energy transferred to the leaf surface. Thus, a supporting rigid substrate such as a wall on which the plant climbs (a typical support for *H. helix*, Fig. S6a, ESI†) may facilitate that more kinetic energy translates into contact electrification (and not elastic deformation of the leaves petiole). We analyzed thus the wind-speed-dependent voltage and current signals using a supporting panel (overview and characteristics of different panel materials are given in Fig. S6b and S6c, ESI†). The panel (Fig. 4k) holds eight c–u pairs of two *H. helix* plants. Fig. 4j shows that the voltage and current signals and the average power scale with the windspeed reaching amplitudes up to ~10 V and ~1 μA (10 μW power peaks and the mean power is 0.26 μW at highest wind speed).

Although harvesting by a few leaves is sufficient to drive low-power electronics, the power output of solely mechanical energy conversion could be further upscaled using (a) more leaf-pairs (a simulation of the behavior of signals from up to 1000 leaves in Fig. S7 (ESI†) suggests the scalability using multiple leaves of the same plant to increase the energy output); (b) using higher contact areas as suggested by Fig. 4d; and (c) by achieving a more effective c–u contact as function of leaf orientations and support.

Thus, also without rectifying the single signals such as by installing a diode bridge at each leaf (which was done in our previous prototypes[5,23]), here, energy harvesting with positive power balance was possible. The model in Fig. S7 (ESI†) that estimates how multiple signals generated in the same plant (and our experiments) suggests that the more leaves generate electricity, the higher is the final energy harvested also when signals generated on the same plant partially compensate if a positive spike should occur simultaneously with a negative spike of another leaf.

However, at still air and very low wind speeds, the system would not provide the same energy. Other effects occurring outdoor like wetting of the leaf surface (during rain periods) will affect the signal transiently even if it recovers after leaf-drying (see effect of leaf-wetting on mechanical energy conversion, Fig. S8, ESI†). The limitations of a single energy source could be overcome by realizing multiple independent and complementary energy conversion modes in plants.

Plant-enabled RF energy harvesting and receiving antenna features

Indeed, a further opportunity for augmenting the overall power output and providing complementary multi-energy system is

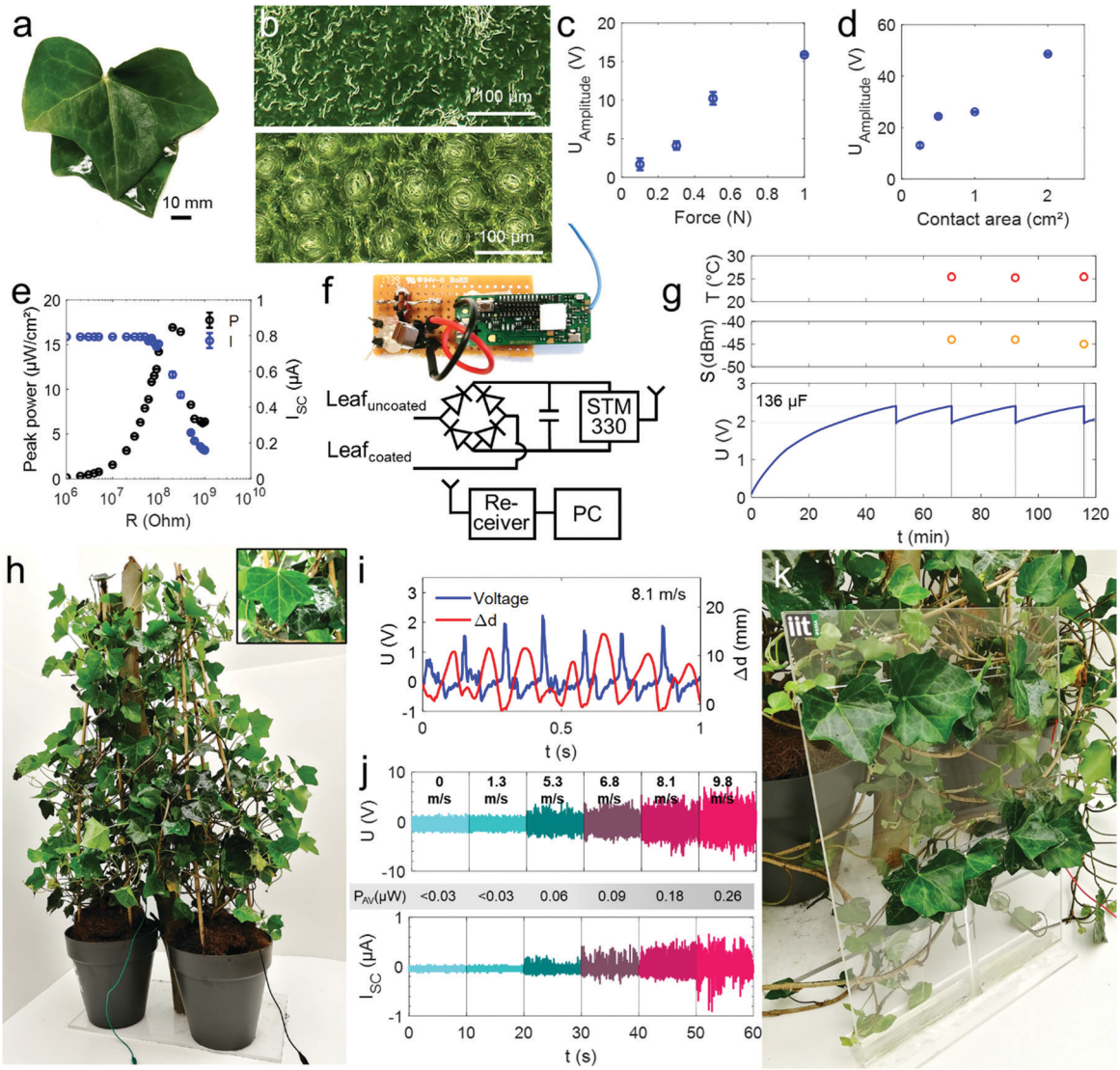

Fig. 4 Realization of mechanical energy harvesting in epicuticular coated climber *H. helix*. (a) Photograph of a *H. helix* c–u leaf pair. (b) Microscopy images representing stomatal density on adaxial and abaxial leaf surface. (c) and (d) Voltage amplitude generated by a *H. helix* c–u leaf pair as function of the impact force (@ contact area 0.25 cm^2) and the contact area (@1 N impact force), respectively (10 Hz stimulus). Data points and error bars represent mean and standard deviations of 100 impacts of the c–u pair per data point. Error bars in (d) are smaller than the symbol size. (e) Peak power analysis of a *H. helix* c–u leaf pair as function of load of resistance considering mean and standard deviations of 100 voltage and current peaks data point. Error bars representing standard deviations are smaller than the symbol size. (f) Circuit overview that was used in (g). (g) Wirelessly transmitted data packets with temperature measurements and signal strength powered by a c–u leaf pair (@1 N, 30 Hz mechanical stimulation). (h) Typical arrangement for *H. helix* wind energy harvesting in which multiple c–u leaf pairs are realized from two separately potted plants. (i) Correlation of voltage signal and the distance between the coated and uncoated leaves in a *H. helix* c–u leaf pair fluttering in air-flow. (j) Voltage and short circuit current generated by eight c–u pairs under wind excitation. The average power (P_{AV}) is given calculated by multiplying the root mean square of the voltage and current signals. Unidirectional leaf pairs were realized by fixing two branches of the two *H. helix* on a support panel as shown in (k).

providing a second energy source by the same plant, ideally without additional modification. Plants were previously suggested for radio reception and transmission.[46,47]

We thus analyzed the received spectrum when *H. helix* is used as a receiving antenna in an outdoor environment with ambient RF pollution (Fig. 5a). The power spectrum analysis shows that the plant receives signals at multiple frequencies: 100 to 800 kHz, low and medium frequency radio communication; at 87–107 MHz, ultra-high frequency FM broadcast radio stations; at ~800 MHz, likely related to Global System for Mobile Communications (GSM); 2.1–2.2 GHz range, fourth generation (4G) broadband cellular network showing broad range RF reception.

We thus slightly modified the harvesting circuit by introducing an earth connection at the rectifier providing a potential difference so that the plant can act as vertical receiver of a Marconi-antenna configuration (Fig. 5b). Indeed, the charging kinetics of a 68 µF capacitor with and without connecting the circuit to two *H. helix* (height ~120 cm) suggests that the signals received by the plant can be converted and stored without the need of any further modifications of the plant.

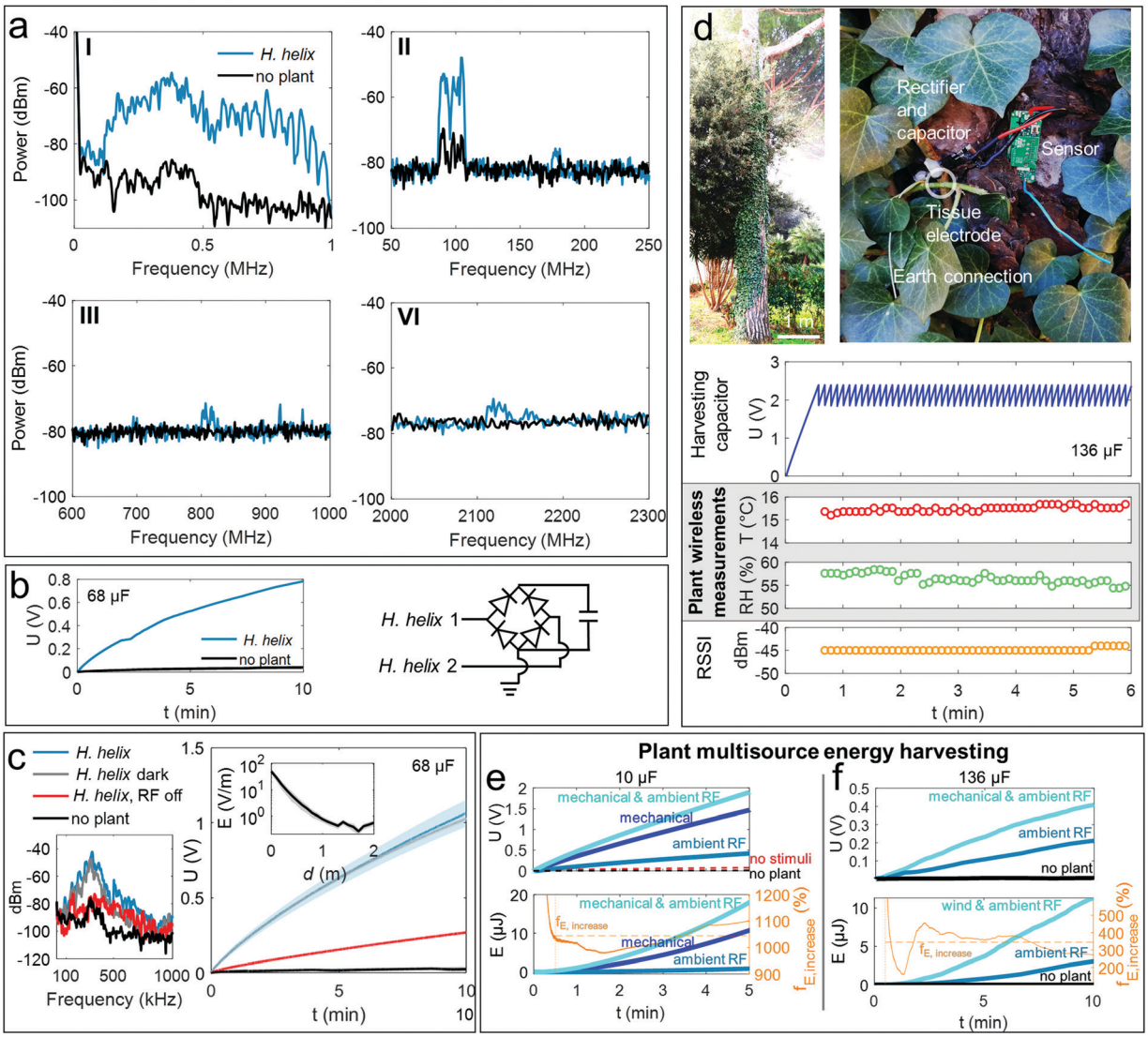

Fig. 5 Plant based RF energy harvesting and multisource wind-RF energy harvesting. (a) and (b) overview of the frequencies received by an *H. helix* acting as antenna outdoor (*e.g.*, @100 MHz, center frequency of nearby radio emitter), circuit and charging curve of a 68 μF capacitor relative to these signals, respectively indicating potential to transduce RF radiation into electricity. (c) Exposure of *H. helix* in dark and light conditions to a switchable RF source resulting in a received main frequency ~400 kHz-center when the RF source is on, when off, the peak diminishes. The capacitor charging curves (68 μF) show RF-source and plant-dependent energy harvesting by *H. helix*. The inset shows the electric field strength as function of distance from the RF source, energy harvesting was performed in ~1 m distance, further details in Fig. S9 (ESI†). The curves are averages from 4 to 7 repetitions per measurement conditions, the filled areas behind the curves represent the standard deviation. For some measurements the standard deviation is about the linewidth. (d) Demo of a plant-powered sensing and wireless data packet transmission using a modified commercial sensing system in an outdoor environment with a *H. helix* growing on a pine tree, charging of a 136 μF capacitor powering sensor and transceiver unit. The plant powers a humidity/temperature sensor and wireless data transmission and fifty measurements and transmissions of the signal strengths are given. (e) Multisource (mechanical and RF) energy harvesting with a c–u *H. helix* pair of two small *H. helix* plants (35 cm height) selectively exposed to ambient RF and/or mechanical energy (controlled 1 N, 10 Hz stimulus). The upper plot shows the voltage *U* of the 10 μF storage capacitor; the lower plot shows the energy *E* accumulated in the capacitor used to calculate the enhancement achieved by multimodal energy harvesting when compared to RF as single source, $f_{E,increase}$, orange line. The dashed orange line indicates the average enhancement of 1040% over the measurement period (calculated excluding the first 30 seconds in which values close to zero lead to an overestimation of $f_{E,increase}$). (f) Multisource wind and RF plant energy harvesting using two large *H. helix* (120 cm height) and eight leaves fixed to a panel (as described in Fig. 4) at wind speed ~8.1 m s^{-1}. The RF spectrum analysis is given in (c). The upper plot shows the voltage *U* of the 136 μF storage capacitor; the lower plot shows the energy *E* accumulated in the capacitor used to calculate the enhancement achieved by multimodal energy harvesting when compared to RF as single source, $f_{E,increase}$, orange line. The dashed orange line indicates the average enhancement of 345% over the measurement period (calculated excluding the first 30 seconds in which values close to zero lead to an overestimation of $f_{E,increase}$).

To further analyze this capability in detail, the *H. helix* was exposed to a fluorescent lighting system acting as a controllable RF source (on–off switching caused a transient peak received by the plant in the kHz range, likely caused by the ballast emission of the fluorescent lighting system[48]) in a phytochamber (25 °C, 40–50% RH). Characteristics of the RF source in terms of

electric field strength and emitted power (6.9 ± 2.3 dBm along plant *z*-axis) are given in Fig. S9a and b (ESI†).

Fig. 5c shows the charging kinetics of a 68 μF capacitor and the main frequencies received by the plants. The maximum instantaneous power transfer under these conditions was 0.25 μW at a matching load resistance of 10–30 MΩ and a maximum current of 0.3 μA by considering the capacitor as the load.

To exclude that the exposure to light/dark conditions has an effect, we measured the capacitor charging and frequency spectrum when *H. helix* was fully covered with a lightproof cloth (Fig. 5c, grey line *H. helix* dark). In addition, to exclude any effects of the circuit components such as the cables for connecting the plant (shielded antenna cables were used), the capacitor charging of the circuit with all cables but without plants was measured (Fig. 5c, black line, no plant). Exposure to darkness did not affect charging and processes related to photosynthetic activity expectedly do not influence the plant-driven charge accumulation from RF energy. The capacitor charging without plant is marginal confirming that the plant is the main receiving antenna.

Interestingly, obstructing ion mobility and conduction by naturally drying the tissue eliminates the capability to charge the capacitor (Fig. S10a, ESI†). The Bode plots of the tissue impedance and phase shift analyzed up to a frequency of 1 MHz show the typical behavior of electrolyte-based conductors (Fig. S10b, ESI†) signifying that tissue ion motion is caused over a large frequency range. Ions for receiving RF signals are also used in ionic liquid- and water-based antennas.[49]

Varying the distance of the *H. helix* from the RF source influences the capacitor charging kinetics (Fig. S9c, ESI†) as the power and the field strength (Fig. S9a and b and inset in Fig. 5c, ESI†) expectedly decrease with the distance from the source. Comparing the emitted power of the RF source and the instantaneous power charging the capacitor $P_{\mathrm{cap,charging}}$ provided by the plant suggests a specific efficiency of 2.2×10^{-3}% in this experiment of the plant converting the RF signal into electricity. The harvesting circuit operates at an efficiency of ~1% comparing plant-received power and $P_{\mathrm{cap,charging}}$.

Even if the conversion efficiency is significantly lower than for tuned RF harvesting systems,[50] the simplicity of realization and marginal material consumption in our case makes the system attractive for combination with other plant-based energy sources.

Plant-powered outdoor wireless sensing

An interesting application scenario is exploiting the plants of urban vegetation for powering battery-free, environmental sensing. We thus modified a commercial sensor and wireless transceiver by the plant-charging circuit shown in Fig. 5b and connected it to a *H. helix* growing on a pine tree in the front yard of a multifamily residence in a suburb of Pisa, Italy, (Fig. 5d) using the house's ground connection as potential difference.

Fig. 5d shows the plant's charging of a 136 μF capacitor powering the sensor node. The plant autonomously powers the temperature and humidity sensing and wireless transmission of the data telegrams shown in Fig. 4d.

Each measurement requires ~75 μC and the average time required to harvest these charges is about 6 seconds in this configuration. Fig. S11a–i (ESI†) shows that the 136 μF capacitor driving the sensing unit is only sufficiently charged when a plant is connected to the circuit and, importantly, that charging is species-dependent.

Analysis of the received signals, charging dynamics, and spectrum analyses of multiple species are given in Fig. S11a–i (ESI†). The results suggest that that different species are suitable to harvest energy from electromagnetic noise and radiation at frequencies from the super low frequency mains radiation (50 Hz) to higher frequencies such as here a peak at 657 kHz related to a MW radio emitter in 8 km distance. A high contribution of the energy harvested in the urban scenario is due to 50 Hz mains radiation (99.9% of energy accumulated and about 0.1% was related to other ambient RF pollution, Fig. S11j. ESI†) rendering the system in particular suitable for energy harvesting nearby buildings.

The average instantaneous power output with the *H. helix* during the outdoor experiments was 6.8 μW and 10.5 μW using a pine tree, respectively.

Enhancement of energy accumulation by simultaneous wind and RF energy harvesting

We then proved that both energy conversion modes (mechanical and RF) can be complementary and simultaneously used. Therefore, a controlled experimental setup was exploited that enables to selectively switch between RF exposure and mechanical excitation. A c–u leaf pair realized in two small *H. helix* plants (30 cm height) was mechanically stimulated at controlled frequency (10 Hz) by a linear actuator in a Faraday cage. Ambient RF exposure was controlled by adding/removing the electromagnetic shielding.

Fig. 5e shows capacitor charging in terms of voltage and accumulated energy by the plants under different conditions. The results confirm that both energy sources can be independently and simultaneously harvested. Moreover, when RF and mechanical stimulation are simultaneously applied, the signals add up leading to faster capacitor charging using the same rectifying circuit and tissue electrode.

The overall enhancement in the accumulated energy using the plant to convert both, mechanical and ambient RF energy in this experiment is 10.4-fold (or 1040%) compared to only RF energy harvesting.

We then tested a larger *H. helix* (120 cm) exposed air flow/wind excitation and RF emitted by the fluorescent lighting system of the phytochamber. Fig. 5f shows the charging dynamics of a 136 μF capacitor under RF and wind stimulation and the energy accumulated in the capacitor. The data suggests an enhancement of the accumulated energy of 345% compared to RF-only harvesting under the experimental conditions.

The energy accumulation and possible enhancement is thus expectedly dependent on factors like the available RF and mechanical energy, the plant properties, as well as the circuit like the capacitance of the storage capacitor. Yet, the results

suggest that energy accumulation can be enhanced at least up to 1000% compared to single RF energy harvesting.

Under outdoor conditions, not only the wind speed but also other weather conditions, for example humidity will further affect the energy output (as suggested by the effects of humidity on mechanical energy conversion of a c–u pair given in Fig. S8, ESI†). RF energy harvesting may be less affected by weather which is, next to signal augmentation, another benefit of multisource energy harvesting.

Table S1 (ESI†) puts the harvesting approach presented here in the context of other plant-hybrid devices. Whereas the power metrics are in the range of the other methods, they could be further upscaled and this paper describes the only multisource approach so far. Our system already powers commercial sensor nodes using single plants.

Additionally, the plant-based energy conversion could be further combined with other existing plant energy harvesting and sensing approaches reported in Table S1 (ESI†) to extend multimodal capabilities enabled by interfacing engineered materials and electronics with living plants. To further validate such technologies, additional application-relevant and in particular outdoor investigations are crucial.

Conclusions

Living plants provide structures and materials that enable to convert different environmental energy sources into electricity. Here, we have presented the first complementary multi-energy harvesting systems exploiting the intrinsic properties of the same plant to convert wind and RF energy.

Using the leaf as energy converter, electrode, and cable at the same time reduces modifications required for energy harvesting. A single electrode in the tissue and an epicuticular coating, harmless for the plant, are the only required modifications of the plants.

Combining wind and RF energy harvesting led to up to 1040% enhancements in the overall energy accumulation. The electricity generated by plants from single or combined sources could power a wireless sensor node, also using vegetation outdoor.

Our results suggest that upscaling of wind energy harvesting is plausible using more leaves and increasing the effective contact area. While the application of the coating which enhanced wind energy harvesting is simple, how modifying plants outdoor in unstructured environments, and how, *e.g.*, weather conditions affect the performance will require further investigations.

Despite that, already few leaves and single plants may provide sufficient power for IoT devices like wireless sensors and the plant-hybrids presented here could lead to new power sources especially suitable for application scenarios where low-power but eco-friendly complementary energy sources are required such as in environmental and agricultural sensing.

Author contributions

F. M. developed the idea, performed the experiments, and wrote the manuscript. F. M., A. M., and B. M. designed experiments. F. M., A. M., F. V., G. Z., and M. C. analysed the data and wrote the manuscript. F. M. wrote the manuscript with contributions of all authors. All authors contributed equally in revising the manuscript.

Conflicts of interest

There are no conflicts to declare.

Acknowledgements

This work was funded by the project GrowBot, the European Union's Horizon 2020 Research and Innovation Programme under Grant Agreement No. 824074.

Notes and references

1 F. Meder, I. Must, A. Sadeghi, A. Mondini, C. Filippeschi, L. Beccai, V. Mattoli, P. Pingue and B. Mazzolai, *Adv. Funct. Mater.*, 2018, **28**, 1806689.
2 Y. Jie, X. Jia, J. Zou, Y. Chen, N. Wang, Z. L. Wang and X. Cao, *Adv. Energy Mater.*, 2018, **8**, 1703133.
3 D. W. Kim, S. Kim and U. Jeong, *Adv. Mater.*, 2018, **30**, 1804949.
4 H. Wu, Z. Chen, G. Xu, J. Xu, Z. Wang and Y. Zi, *ACS Appl. Mater. Interfaces*, 2020, **12**, 56060–56067.
5 F. Meder, M. Thielen, A. Mondini, T. Speck and B. Mazzolai, *Energy Technol.*, 2020, **8**, 2000236.
6 T. T. S. Lew, V. B. Koman, P. Gordiichuk, M. Park and M. S. Strano, *Adv. Mater. Technol.*, 2020, **5**, 1–12.
7 M. H. Wong, J. P. Giraldo, S. Kwak, V. B. Koman, R. Sinclair, T. Thomas, S. Lew, G. Bisker, P. Liu and M. S. Strano, *Nat. Mater.*, 2017, **16**, 264–272.
8 J. J. Kim, L. K. Allison and T. L. Andrew, *Sci. Adv.*, 2019, **5**, eaaw0463.
9 J. P. Giraldo, M. P. Landry, S. M. Faltermeier, T. P. Mcnicholas, N. M. Iverson, A. A. Boghossian, N. F. Reuel, A. J. Hilmer, F. Sen, J. A. Brew and M. S. Strano, *Nat. Mater.*, 2014, **13**, 400–408.
10 J. J. Kim, R. Fan, L. K. Allison and T. L. Andrew, *Sci. Adv.*, 2020, **6**, 1–10.
11 T. T. S. Lew, M. Park, J. Cui and M. S. Strano, *Adv. Mater.*, 2021, **33**, 1–11.
12 J. Jiang, S. Zhang, B. Wang, H. Ding and Z. Wu, *Small*, 2020, 16.
13 H. Wu, R. Nißler, V. Morris, N. Herrmann, P. Hu, S. Jeon, S. Kruss and J. P. Giraldo, *Nano Lett.*, 2020, **20**, 2432–2442.
14 C. Diacci, T. Abedi, J. W. Lee, E. O. Gabrielsson, M. Berggren, D. T. Simon, T. Niittyla and E. Stavrinidou, *iScience*, 2021, **24**, 101966.
15 G. Dufil, I. Bernacka-Wojcik, A. Armada-Moreira and E. Stavrinidou, *Chem. Rev.*, 2022, **122**(4), 4847–4883.
16 J. P. Giraldo, H. Wu, G. M. Newkirk and S. Kruss, *Nat. Nanotechnol.*, 2019, **14**, 541–553.
17 T. Thomas, S. Lew, V. B. Koman, P. Gordiichuk, M. Park and M. S. Strano, *Adv. Mater. Technol.*, 2019, **1900657**, 1–12.

18 T. Thomas, S. Lew, R. Sarojam, I. Jang, B. S. Park, N. I. Naqvi, M. H. Wong, G. P. Singh, R. J. Ram, O. Shoseyov, K. Saito, N. Chua and M. S. Strano, *Nat. Plants*, 2020, **6**, 1408–1417.
19 S.-Y. Kwak, J. P. Giraldo, M. H. Wong, V. B. Koman, T. T. S. Lew, J. Ell, M. C. Weidman, R. M. Sinclair, M. P. Landry, W. A. Tisdale and M. S. Strano, *Nano Lett.*, 2017, **17**, 7951–7961.
20 E. Stavrinidou, R. Gabrielsson, K. P. R. Nilsson, S. K. Singh, J. F. Franco-Gonzalez, A. V. Volkov, M. P. Jonsson, A. Grimoldi, M. Elgland, I. V. Zozoulenko, D. T. Simon and M. Berggren, *Proc. Natl. Acad. Sci. U. S. A.*, 2017, **114**, 2807–2812.
21 E. Stavrinidou, R. Gabrielsson, E. Gomez, X. Crispin, O. Nilsson, D. T. Simon and M. Berggren, *Sci. Adv.*, 2015, **1**, e1501136.
22 W. Li, N. Matsuhisa, Z. Liu, M. Wang, Y. Luo, P. Cai, G. Chen, F. Zhang, C. Li, Z. Liu, Z. Lv, W. Zhang and X. Chen, *Nat. Electron.*, 2021, **4**, 134–142.
23 F. Meder, S. Armiento, G. A. Naselli and M. Thielen, *Bioinspir. Biomim.*, 2021, **16**, 55009.
24 H. Deng, Z. Chen and F. Zhao, *ChemSusChem*, 2012, **5**, 1006–1011.
25 M. Helder, D. Strik, H. V. M. Hamelers, A. J. Kuhn, C. Blok and C. J. N. Buisman, *Bioresour. Technol.*, 2010, **101**, 3541–3547.
26 D. P. B. T. B. Strik, H. V. M. H. Bert, J. F. H. Snel and C. J. N. Buisman, *Int. J. Energy Res.*, 2008, **32**, 870–876.
27 Y. Xu, Y. Lu and X. Zhu, *ACS Sustainable Chem. Eng.*, 2021, **9**, 1099–1104.
28 V. Flexer and N. Mano, *Anal. Chem.*, 2010, **82**, 1444–1449.
29 T. Miyake, K. Haneda, N. Nagai, Y. Yatagawa, H. Onami, S. Yoshino, T. Abec and M. Nishizawa, *Energy Environ. Sci.*, 2011, **4**, 5008–5012.
30 N. Mano, F. Mao and A. Heller, *J. Am. Chem. Soc.*, 2003, **125**(21), 6588–6594.
31 C. P. Souza, F. B. S. Carvalho, F. A. N. Silva, H. A. Andrade, N. D. V. Silva, O. Baiocchi and I. Müller, *Int. J. Distrib. Sens. Networks*, 2016, **12**, 9383765.
32 C. Himes, E. Carlson, R. J. Ricchiuti, B. P. Otis, B. A. Parviz and A. Overview, *IEEE Trans. Nanotechnol.*, 2010, **9**, 26–29.
33 U. M. R. Mogili and B. B. V. L. Deepak, *Procedia Comput. Sci.*, 2018, **133**, 502–509.
34 R. Shogren, D. Wood, W. Orts and G. Glenn, *Sustain. Prod. Consum.*, 2019, **19**, 194–215.
35 E. M. Izhikevich, *Dynamical systems in neuroscience*, MIT Press, 2007.
36 H. Chen, Y. Xu, J. Zhang, W. Wu and G. Song, *Nanoscale Res. Lett.*, 2018, **13**, 346.
37 J. Lowell and A. C. Rose-Innes, *Adv. Phys.*, 1980, **296**, 947–1023.
38 Z. Lin and A. Chi, *Mater. Today*, 2019, **30**, 34–51.
39 D. J. Lacks and T. Shinbrot, *Nat. Rev. Chem.*, 2019, **3**, 465–476.
40 T. H. Yeats and J. K. C. Rose, *Plant Physiol.*, 2013, **163**, 5–20.
41 O. Speck and T. Speck, *Biomimetics*, 2019, **4**, 26.
42 M. Köhler, *Urban Ecosyst.*, 2008, **11**, 423–436.
43 Y. Bai, H. Jantunen and J. Juuti, *Adv. Mater.*, 2018, **30**, 1–41.
44 P. Thainiramit, P. Yingyong and D. Isarakorn, *Sensors*, 2020, **20**, 1–20.
45 Y. Bai, H. Jantunen and J. Juuti, *Front. Mater.*, 2018, **5**, 1–10.
46 K. Ikrath, W. Kennebeck and R. T. Hoverter, *IEEE Trans. Antennas Propag.*, 1975, **23**, 137–140.
47 K. Skrivseth, US Army Electron. Command, 171AD.
48 G. Schmidt and I. Berta, *Int. J. Plasma Environ. Sci. Technol.*, 2011, **5**, 84–92.
49 C. Hua, Z. Shen and J. Lu, *IEEE Trans. Antennas Propag.*, 2014, **62**, 5968–5973.
50 M. Cansiz, D. Altinel and G. K. Kurt, *Energy*, 2019, **174**, 292–309.

